Beat-to-beat interplay of heart rate, ventricular depolarization, and repolarization

György Kozmann, DSc,[a,b,*] Kristóf Haraszti, MSc,[b,c] István Préda, MD, DSc[d,e]

[a]Department of Electrical Engineering and Information Systems, University of Pannonia, Veszprém, Hungary
[b]Department of Biomedical Engineering, Research Institute for Technical Physics and Materials Science of the Hungarian Academy of Sciences, Budapest, Hungary
[c]IQSYS Computing, member of Hungarian Telekom Group, Budapest, Hungary
[d]Department of Cardiology, State Health Center, Budapest, Hungary
[e]Cardiovascular Center, Semmelweis University, Budapest, Hungary

Abstract

To improve malignant arrhythmia risk stratification, the causal and random components of spatiotemporal dynamics of heart rate (RR distances), ventricular depolarization sequence, and repolarization disparity were studied based on body surface potential map records taken for 5 minutes, in resting, supine position on 14 healthy subjects (age range, 20-65 years) and on 6 arrhythmia patients (age range, 59-70 years). Beat-to-beat QRS and QRST integral maps, Karhunen-Loève (KL) coefficients, RR, and nondipolarity index time series were computed. Tight relationship was found between RR and QRS integrals in healthy subjects with less association in arrhythmia patients. Tight KL-domain multiple linear association ($r^2 > 0.72$) was found between the QRS and QRST integral dynamics (ie, depolarization sequence and repolarization disparity). Beat-to-beat probability of the generation of significant nondipolarity index spikes was proportional to the QRST KL-component standard deviations (SD_i) and inversely proportional with the mean dipolar KL components (M_i) of the average QRST integral map.
© 2010 Elsevier Inc. All rights reserved.

Keywords: Repolarization disparity; Depolarization sequence; Body surface potential maps; Arrhythmia vulnerability; Heart rate variability

Introduction

Ventricular fibrillation is the most common cause of sudden cardiac death. According to experimental and theoretical studies, the biophysical substrate of ventricular fibrillation is strongly connected to the structural and/or dynamical repolarization heterogeneity.[1] In the past few decades, intensive research efforts tried to elaborate simple electrocardiogram (ECG)-based noninvasive methods of repolarization heterogeneity assessments.[2] We refer to the methods based on the evaluation of QT dispersion and QT variability (eg, Berger et al,[3] Atiga et al,[4] and Burattini and Zareba[5]), the measures of heart rate (HR) variability,[6] the heart rate turbulence parameters, or the alternating T-wave components in ECG.[7-9]

In our view, these risk evaluation methods are suboptimal because they do not address statical and dynamical spatiotemporal properties of ventricular repolarization dispersion directly and do not exploit all the signal-information accessible noninvasively.[1,10]

In this study, we used the QRST integrals of body surface potential maps instead of conventional ECG leads to grasp the whole repolarization disparity information available on the thoracic surface. The roots of our approach rely on the early experimental work of Abildskov others (eg, Abildskov et al[11] and Hubley-Kozey et al[12]). Theoretically, the relationship of QRST integral maps and repolarization disparity was proved by Plonsey[13] and Geselowitz.[14]

In our approach, both averaged and beat-to-beat QRST integral maps were computed to extend the utility of the beat-to-beat variability concept of Berger et al.[3] In the first part of this article, linear models are used to characterize the interplay of the depolarization sequence and RR interval and the repolarization disparity versus depolarization sequence.

---

* Corresponding author. Department of Electrical Engineering and Information Systems, University of Pannonia, H-8201 P.O. Box 158, Veszprém, Hungary.

E-mail address: kozmann@irt.vein.hu

In the second part, the necessary conditions of frequent highly heterogeneous repolarization disparity formations are discussed based on our learning set.

Materials and methods

In this study, we heavily rely on theoretical studies characterizing the relationship of ventricular depolarization and QRS integral maps as well as on the results describing the relationship of repolarization disparity and QRST integral maps.

QRS integral maps versus depolarization sequence

The QRS integral of an arbitrary unipolar chest surface ECG signal $\phi(P,t)$ can be expressed at an arbitrary body surface point P by the volume integral of the $\mathbf{i}_m(\mathbf{r})$ "impressed" cellular depolarization current distribution weighted by the $\mathbf{z}(P,\mathbf{r})$ lead vector (Eq. [1]). If the uniform double layer approximation of depolarization wave front prevails (which is frequently assumed), the QRS integral at a point P can be related to the endoepicardial depolarization sequence.[15,16]

$$\int_{QRS}\phi(P,t)dt = c\iiint_{V_s}\mathbf{z}(P,\mathbf{r})\mathbf{i}_m(\mathbf{r})dV_s \qquad (1)$$

where $\mathbf{i}_m(\mathbf{r})$ is impressed current due to cellular depolarization; V_s, volume of sources (myocardium); $\mathbf{r}$, position vector; and c, constant.

The QRS integral maps computed in each measuring point by (Eq. [1]) characterize the depolarization sequence of the ventricles in details.

QRST integral maps versus repolarization dispersion

According to Plonsey and Geselowitz, the QRST integrals computed in an arbitrary thoracic point P are associated with the volume integral of the $\nabla\mu(\mathbf{r})$ gradient of the $\mu(\mathbf{r})$ action potential area, weighted by the $\mathbf{z}(P,\mathbf{r})$ lead vectors (the same as in Eq. [1]) corresponding to dV_s volume elements (Eq. [2]). By evaluating for each thoracic point (Eq. [2]), QRST integral maps can be computed. As long as the spatial distribution of action potential areas is temporally stable within the myocardium, QRST integrals (QRST integral maps) are identical in the subsequent heart cycles and invariant to the depolarization sequence.[14] Changes of the length and/or the shape of action potentials influence the amplitude of QRST integrals at an arbitrary body surface point P. Consequently, the beat-to-beat application of QRST integral maps provides a noninvasive tool that can be used to study the spatiotemporal properties of repolarization dispersion.

$$\int_{QRST}\phi(P,t)dt = -k\iiint_{V_s}\mathbf{z}(P,\mathbf{r})\nabla\mu(\mathbf{r})dV_s \qquad (2)$$

where $\mu = \int_{QRST}[\phi_m(\mathbf{r},t) - \phi_{mr}(\mathbf{r})]dt$ (ie: action potential area); $\phi_m(\mathbf{r},t)$, membrane potential at time t; $\phi_{mr}(\mathbf{r})$, membrane resting potential at an intraventricular point $\mathbf{r}$; k, constant.

It is important to note that the heart-to-body surface projection rules in Eqs. (1) and (2) are identical; therefore, the beat-to-beat organ-level dynamic changes in the depolarization sequences or in the repolarization disparities are directly comparable by the body surface QRS and QRST integral maps.

Measurements and preprocessing

In our study, we assessed, by noninvasive beat-to-beat measurements, the RR fluctuations and the spatiotemporal depolarization and repolarization dynamics by means of long body surface potential mapping (BSPM) records taken on 14 healthy male and female subjects (6 males and 8 females aged 20-65 years; mean, 36 years, all with normal ECG and without a history of cardiovascular disease) and on 6 arrhythmia patients (aged 59-70 years; 4 males and 2 females; mean, 63.5 years), all with implanted cardioverter defibrillator, history of myocardial infarction, resuscitation, supraventricular tachycardia, or positive electrophysiological test. In 4 patients, ejection fraction was 0.35 or less; in 2 patients, ejection fraction was 0.48 and 0.69, respectively. In 2 cases, QRS was more than 120 milliseconds. All records were taken continuously, for a period of 5 minutes, in resting, supine position.

All healthy volunteers and arrhythmia patients gave an informed consent for body surface mapping, and the study protocol had the prior approval of the Cardiovascular Research Group.

Unipolar ECG leads were recorded in 64 chest positions by the BioSemi Mark-8 System in accordance with the electrode layout suggested in Amsterdam.[17,18] (The layout is a subset of the 12-row × 16-column uniform lead arrangement suggested in Salt Lake City.) Data processing started with the identification of individual beats, high-precision determination of QRS fiducial points for each beat, and classification of QRS patterns. Time instants of the most negative derivative of the QRS waves were used as fiducial points. Subsequently, Q_{on}, S_{end}, and T_{end} points were manually marked based on the "papillon-diagram," that is, the diagram of time-aligned averaged superimposed unipolar leads. After a linear baseline adjustment from the 64 recorded ECG signals, ECG signals were estimated in 128 other chest locations of the 192-lead regular measurement point arrangement introduced at the Cardiovascular Research and Training Institute, Salt Lake City. The procedure of signal estimations followed the principle of root-mean-square error minimization suggested by Lux et al.[19] Subsequently, beat-by-beat QRS and QRST integrals were computed from the resultant dataset of the 192-lead system. The 64-to-192-lead expansion improved the fidelity of the QRS and QRST integral map estimations and made it possible to characterize the beat-to-beat variations in terms of bioelectrical processes and parameters, such as ventricular depolarization sequence and repolarization disparity. In the first step, the beat-to-beat depolarization sequence and repolarization disparity interplay was computed exclusively for sinus beats; subsequently, the computations were repeated for all the beats.
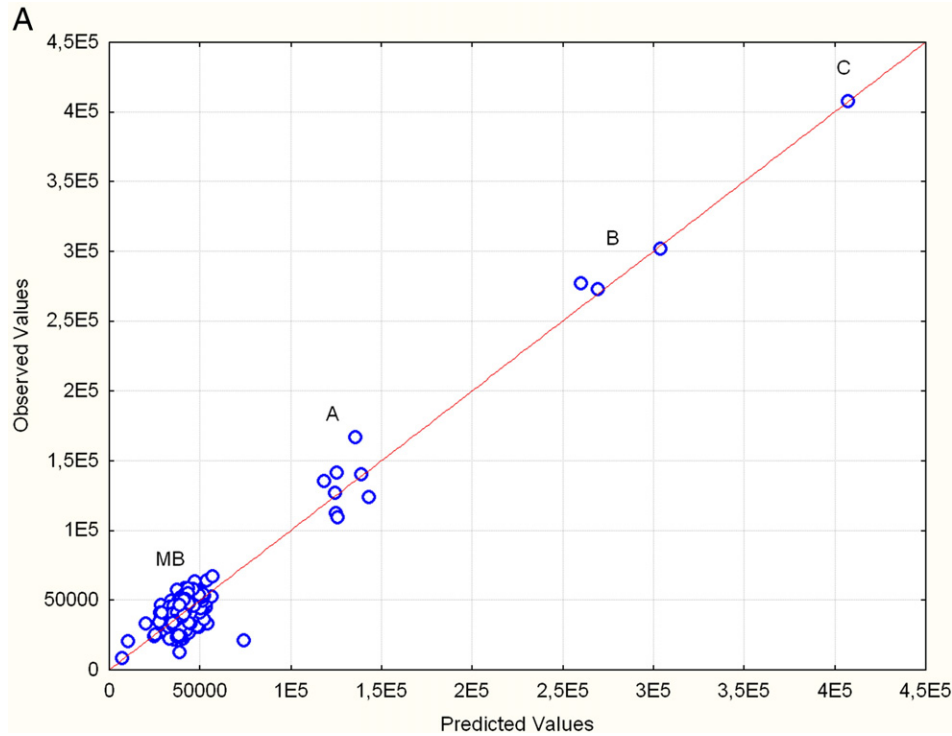
Fig. 1. Typical example of the observed versus predicted KL component values computed by the **T** matrix for all the beats of an ARR patient with frequent premature beats. MB stands for the cluster of majority beats, whereas A, B, and C denote 3 clusters of ectopic beats with different foci (A). Example of majority (MB) and ectopic (type A) QRS and QRST integral map pairs. The left side of the color-coded maps represent the anterior thoracic surface, the right side the back. Red areas represent positive integral values; blue areas show the negative values. The numbers around the maps denote the rows and the columns of the electrode matrix (B). Heart rate (RR) and depolarization sequence (DS) dependence of α (only KL_1QRS coefficients are used to illustrate DS clusters) (C). It is to be observed that different DS patterns largely influence KL(QRS) coefficients (in this example, $KL_1[QRSint]$), but α depends mainly on RR. (Curved lines show iso-α contours.)

Advanced processing methods

The relationship of RR and the depolarization sequence and the relationship of ventricular depolarization sequence and repolarization dispersion were approximated by linear regressional models. The computations were carried out in the 12-D space of Karhunen-Loève (KL) eigenvectors introduced by Lux et al,[20] using the c_i components of (Eq. [3]).

$$c_i = \Phi^T e_i \qquad (3)$$

where Φ^T is integral vector of body surface potentials in the time interval of QRS or QRST, respectively, and e_i, i-th spatial eigenvector of the eigenequation computed from the covariance matrix of a representative learning population.[20]

Heart rate dynamics were assessed by the time series of RR distances. Beat-to-beat spatial repolarization disparity changes (ie, QRST integral map topography changes) were characterized in a concise manner by the beat-to-beat sequence of nondipolarity indices (NDIs) defined in (Eq. [4]). Based on the physical meaning of NDIs, the high NDI values indicate highly fragmented repolarization distribution. According to Abildskov et al, a threshold of an NDI of more than 0.2 indicates pathologic repolarization dispersion.[21] It is to be noted that the series of NDI values provides a concise representation of normal or pathologic

repolarization disparity changes, but their spatial localization is not preserved.

$$NDI = \frac{\sum_{i=4}^{12} c_i^2}{\sum_{i=1}^{12} c_i^2} = \frac{P_{ND}}{P_D + P_{ND}} \qquad (4)$$

where P_D is QRS or QRST integral map signal power represented by the "dipolar" KL components ($i = 1$-3); P_{ND}, QRS or QRST integral map signal power represented by the "non-dipolar" KL components ($i = 4$-12); and RR, KL, and NDI time series were analyzed with the STATISTICA (StatSoft, release 6, Tulsa, OK) program package.

Results

Interdependence of RR time series and QRS integral maps

Because of the varying oxygenated blood demand of the body, the cardiac output is continuously controlled via the regulation of the HR (RR distances) and contractility, which is achieved by the appropriate modulation of spatiotemporal depolarization sequence and repolarization dispersion. Consequently, a tight relationship can be expected between RR and depolarization sequence. Indeed, in our healthy test group, by knowing QRS integral map KL components, the relevant RR distances were adequately predictable with a
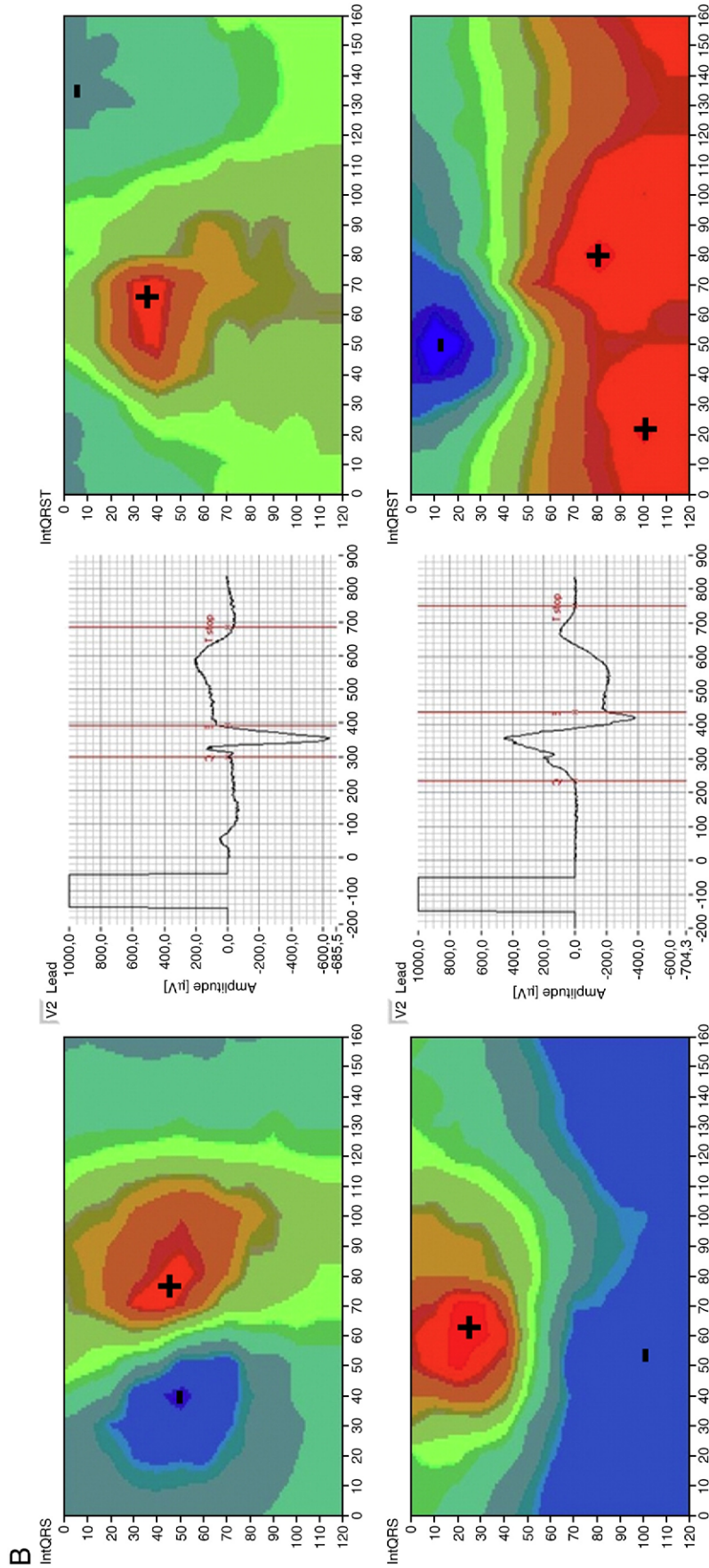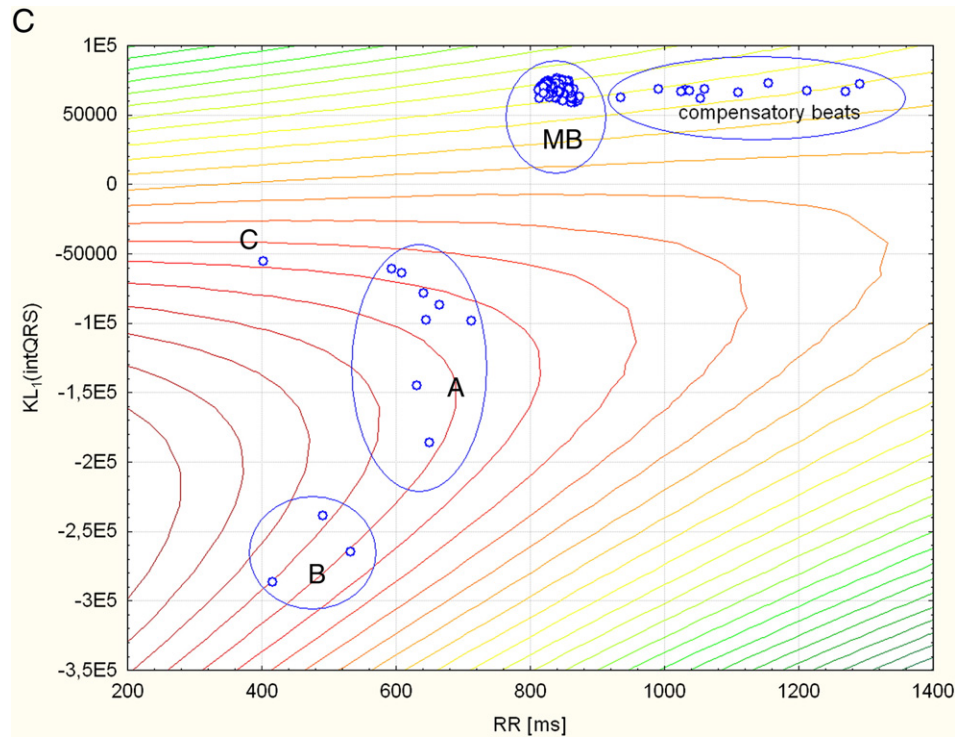
Fig. 1 (*continued*).

Fig. 1 (*continued*).

linear multiple regression equation. The r^2 value (explained variance) in young and older healthy subgroups (H1 and H2) were 0.68 ± 0.10 and 0.57 ± 13.2, respectively, whereas for arrhythmia (ARR) patients, r^2 was 0.34 ± 0.09. Further details are shown in Fig. 1 of the electronic supplement.[1]

Relationship of QRS and QRST integral maps

The personalized functional relationship of within-beat body surface QRS and QRST integral maps (ie, the relationship of depolarization sequence and repolarization disparity) may give a clue to the formation of the arrhythmogenic substrate within the heart due to a pathologic control. Based on our KL domain beat-to-beat QRS and QRST integral map data, multiple linear regression models were used to assess their relationship. This means that we need to identify matrix **T** and vectors **b** and **e** in Eq. (5).

$$\mathbf{KL}(QRST) = \mathbf{T} * \mathbf{KL}(QRST) + \mathbf{b} + \mathbf{e} \qquad (5)$$

where

$$\mathbf{T} = \begin{bmatrix} a_{1,1} & a_{1,2} & \cdots & a_{1,12} \\ a_{2,1} & a_{2,2} & \cdots & a_{2,12} \\ \vdots & \vdots & \ddots & \vdots \\ a_{12,1} & a_{12,2} & \cdots & a_{12,12} \end{bmatrix} \text{ and } \mathbf{b} = \begin{bmatrix} b_1 \\ b_2 \\ \vdots \\ b_{12} \end{bmatrix}$$

where **T** is transformation matrix; $a_{i,j}$, transfer matrix element (regression coefficients); **b**, constant vector (intercept); **e**, residual error vector; **KL**(QRS), 12-D vector of the

QRS integral map KL components; and **KL**(QRST), 12-D vector of the QRST integral map KL components.

The strength of the linear dependence was characterized for each KL parameter separately by the relevant r^2 values. The mean r^2 value of all the 12 individual KL r^2 values in the normal group yielded 0.79 ($r > 0.88$), whereas in the ARR group, the same measure was 0.72 ($r > 0.84$); that is, for the sample sizes available, the strength of linear dependence did not differ significantly in the healthy and ARR groups. The involvement of other variables such as RR or the KL component values of the preceding QRST integral maps did not improve the strength of multiple linear regression.

The above computations were based on record segments without ectopic, compensatory, and/or paced beats. However, according to Fig. 1A, the linear relationship of depolarization sequence and repolarization disparity (in terms of QRS and QRST integrals) persists even if we consider the entire set of sinus, premature, compensatory, and paced beats (A, B, and C clusters of beats with different foci). Fig. 1B shows an example pair of QRS integral map and QRST integral map from the majority group and from the ectopic beat cluster A.

According to Fig. 1C, the linearity does not mean identical and/or fixed orientation of the **KL**(QRS) and **KL**(QRST) vectors. In fact, the α angle spanned by the **KL**(QRS) and **KL**(QRST) vectors in the 12-D space of KL components essentially depends on the RR distance, but the depolarization sequence plays a minor role as well. In case of complete depolarization sequence independence, observation points with identical RR should lie on the same α-contour line.
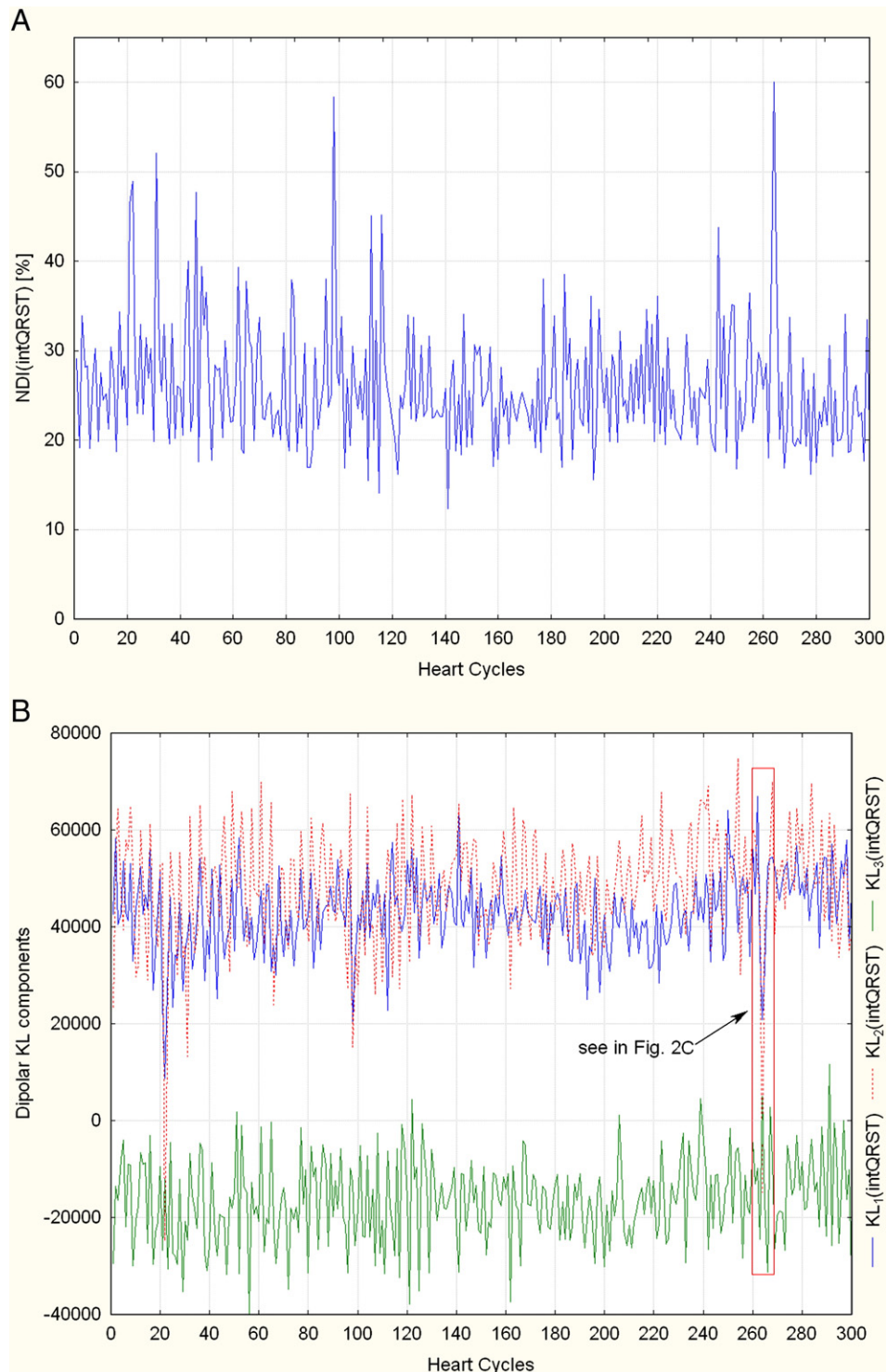
Fig. 2. (A), NDI plot of an ARR patient. B, Time series of KL_1-KL_3 "dipolar" QRST integral map coefficients. Zoomed segment of (B) showing a KL coefficient constellation resulting in NDImax in cycle 264 (C). QRST integral maps in cycle 264, and the cycle preceding and after it (D).

Random components of QRST integral, NDI(QRST)

The spatiotemporal variability of subsequent QRST integral maps was characterized by the SD^2/M^2 (KL amplitude variance over mean KL component energy) values of the QRST integral maps in the normal group ranged between 0.0057 and 0.008 (ie, $0.075 \leq SD/M \leq 0.089$). In the group of ARR patients, the relative variability of the QRST integral maps increased signifi-

cantly, SD^2/M^2 values increased up to 0.021 to 0.069 (ie, $0.14 \leq SD/M \leq 0.26$). An example in terms of KL coefficient scattering plots is shown in Fig. 2 of the electronic supplement.[2]

Fig. 2 shows an example of NDI spike generation. In Fig. 2A, the time series of NDI coefficients are plotted for an ARR patient. In Fig. 2B, the first 3 ("dipolar") KL
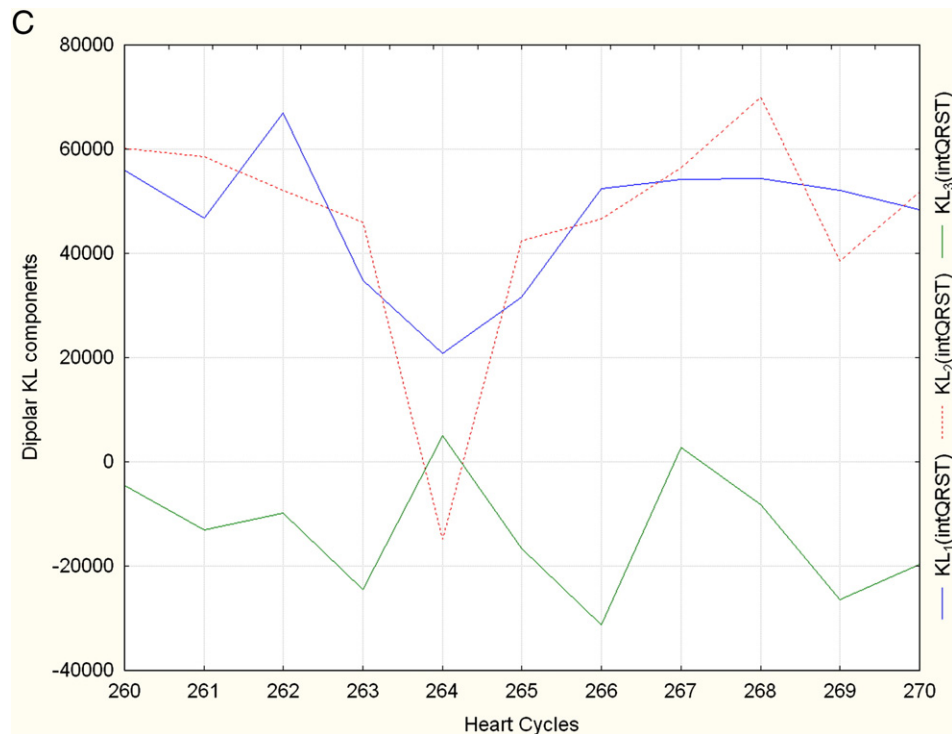
Fig. 2 (*continued*).

components are shown beat-to-beat for cycles 1 to 300. Note that in all 3 KL components, the SD values are relatively large compared with the relevant absolute mean values. Consequently, it is more likely to find cycles where the amplitudes of the first 3 KL components are close to zero (eg, cycle 264 in Fig. 2B, C). In cycles like this, the nondipolar KL components dominate, which causes high-amplitude spikes in NDI plots, according to Eq. (4). In the QRST integral maps, the dominance of the nondipolar KL components[4-12] is the sign of fragmented, nonsmooth spatial distribution with multiple maxima and minima and/or inflections (Fig. 2D).

Judging from the results shown in Fig. 3, the SD/M scattering of the KL components was augmented in ARR patients, compared with the 2 subgroups of healthy subjects. The relatively large random changes in the dipolar KL components significantly influence the pattern of QRST integral maps, revealing large beat-to-beat spatial differences in repolarization disparity distributions (Fig. 2D).

The video supplement[3] shows a 3-dimensional representation example of the random deviations of the subsequent QRST integrals (reconstructed from the KL components) from their mean value in an ARR patient along the unrolled body surface. (The left half of the thoracic surface representation corresponds to the anterior chest surface, the right half to the back. The upper border line is at the height of the clavicular notch, the lower at the umbilicus.)

The fact that the largest deviations in the QRST integrals are often rather far away from the 12-lead ECG measuring points underlines the benefits of the BSPM technique for sudden cardiac death risk assessment.

Discussion

In the interpretation of our results, we did assume that all the dynamic changes in the heart and the circulatory system aim to maintain an optimal matching of the heart to the respiratory and the vascular system under the time-varying demand of the environment.[22-27] According to our estimates in young healthy subjects, the strength of the linear multiple regression of RR and depolarization sequence is tight. However, the coordinated RR and the depolarization sequence modulation slowly decline in healthy older subjects causing a decline in r^2. In parallel with the decline of r^2, a gradual decrease in HR variability parameter SD of RR intervals was observed as well. In the implanted cardioverter defibrillator group, r^2 decreased significantly, in line with a further decrease of the SD of RR intervals.[6]

The results shown in Fig. 1 intended to identify macroscopic bioelectrical sources responsible for elevated repolarization disparity. In sinus-beat time series, Fig. 1 revealed a tight beat-to-beat linear relationship between QRS and QRST integral maps with high r^2 coefficients. The high r^2 value suggests that elevated repolarization disparity mainly originates from the changes in the depolarization sequence. In our learning set, the relationship in the ARR group was almost as tight as in the healthy group. When extending our measurements to all the beats in the records, including sinus beats, ectopic beats with 3 different foci, and even paced beats, the regression

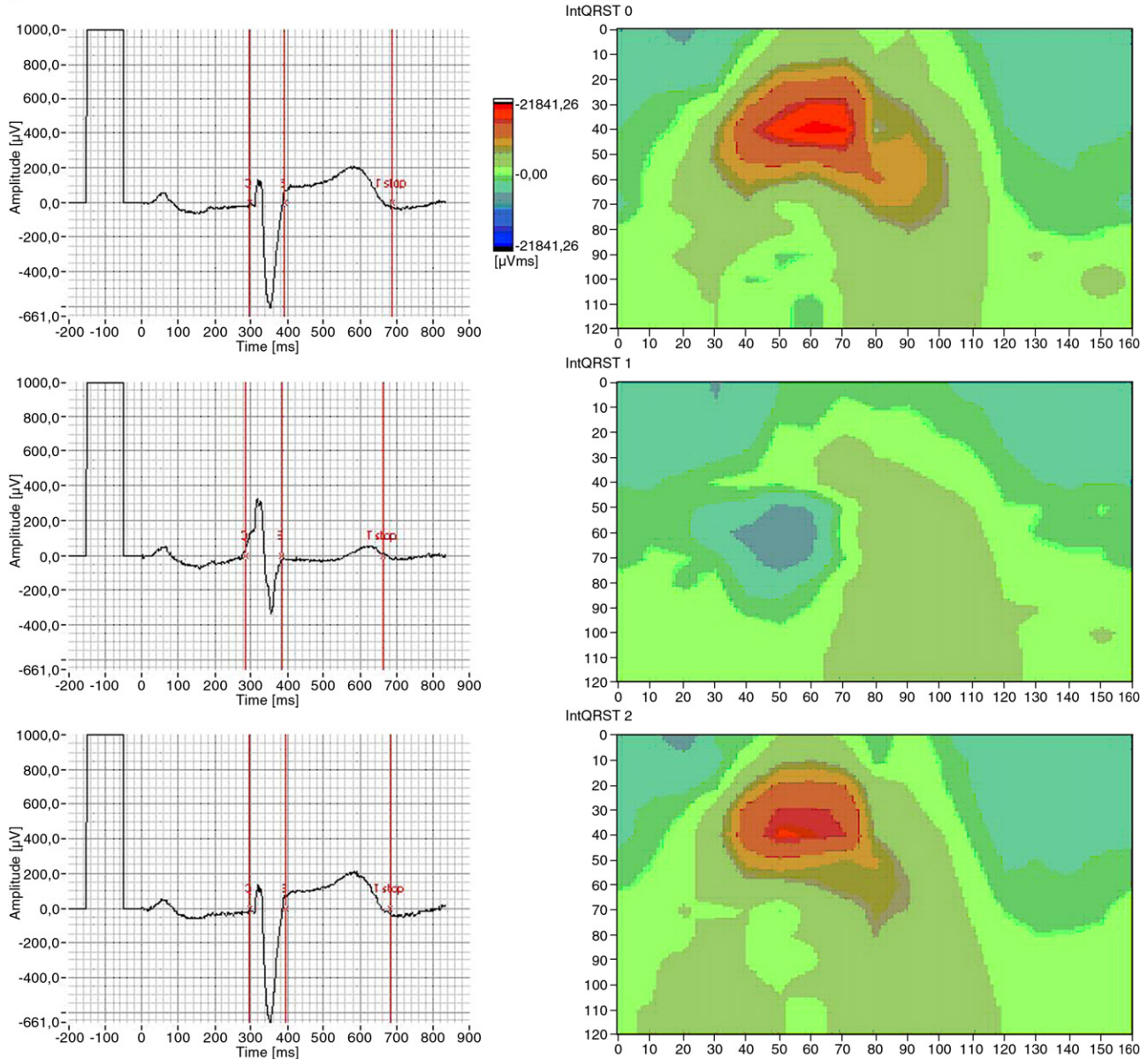³ http://web.t-online.hu/harasztikristof/B2B_dynamic/.

Fig. 2 (continued).

relationship itself did not change; that is, **T** and **b** are unchanged (Fig. 1A). These findings are supported indirectly by the results of other authors.[28,29]

Considering the repolarization disparity versus depolarization sequence relationship approximation (Eq. [5]), all the factors influencing the depolarization sequence should influence the repolarization disparity as well. Based on Eqs. (1) and (2), the cardiac sources of the depolarization sequence (ie, QRS integral maps) and repolarization disparity (ie, QRST integral maps) are different. The findings of Fig. 1C reveal that the integrated effect of elementary source orientation differences is subject to RR cycle length. This is true because cycles with similar RR are lying on nearly identical iso-α lines even if they correspond to ectopic beats of different foci (see cluster elements A and B).

The results detailed in Fig. 2 show examples of features possibly useful when ranking arrhythmia vulnerability. The behavior of the individual 12 KL coefficients does not provide a concise easily interpretable characterization of the beat-to-beat fluctuation of repolarization disparity in the myocardium. However, NDI plots comparing the proportion of the signal power of nondipolar KL components (ie, with multiple positive and negative areas on the chest surface) to the power of all the KL components enhance sensitively the malignant changes of the myocardial heterogeneity.

Our experiences show that frequent NDI spikes manifest only if the KL mean values in dipolar components are low (in absolute value) compared with the relevant SD values, that is, when the "relative scattering" is high. Based on this result, in Fig. 3, a tentative "forbidden region" for the
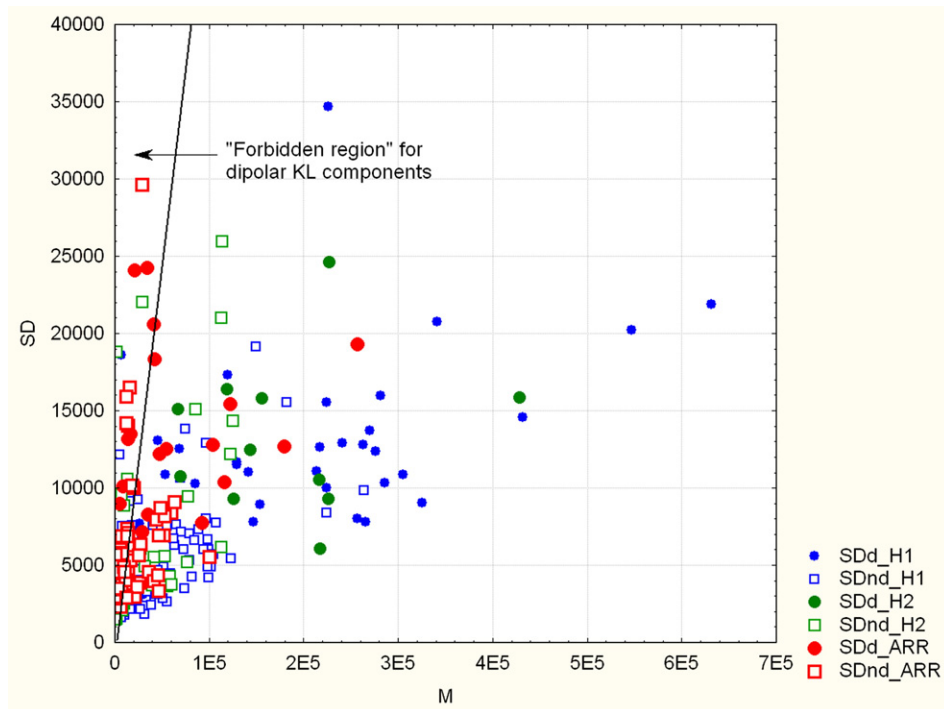
Fig. 3. Scatter diagram of all the KL component (*M*, SD) value pairs of healthy (H1 and H2) subjects and arrhythmia (ARR) patients. Blue symbols stand for the dipolar (d) and nondipolar (nd) SD components of H1 healthy subjects, green symbols for the d and nd SD components of H2 healthy subjects, and red symbols for the d and nd SD components of ARR patients. The tentative "forbidden region" for the location of dipolar components is located left to the heavy black straight line.

dipolar KL mean values is depicted in the *M*-SD plot of our learning sets. Because beat-to-beat KL components can be considered as independent Gaussian random variables, the necessary conditions of NDI spike formations are fulfilled randomly in the subsequent cycles depending on the SD/*M* ratio.[30]

Conclusions

Beat-to-beat analysis of RR distances and QRS and QRST integral maps provides an insight into the ventricular depolarization sequence and repolarization disparity dynamics in healthy subjects and even in malignant arrhythmia patients. Most importantly, we have found a consistent tight association between the depolarization sequence (QRS integral) dynamics and repolarization disparity (QRST integral) dynamics. According to our beat-to-beat statistical model, repolarization disparity is dominantly determined by the properties of depolarization sequence.

In each cardiac cycle, the multilead (BSPM) measurement approach provides unique details on the dynamics of arrhythmia-prone status development. The beat-to-beat evaluation of NDI draws our attention to the importance of the large variability in the KL domain dipolar components, which have an important impact on the formation of cycles with significantly elevated repolarization disparity.

Obviously, the low number of cases in both of our learning sets limits the immediate clinical applicability of our conclusions. From this aspect, we consider this study as a preliminary, conceptual one; the elaboration of reliable

clinical decision support solutions needs a large number of validated measurements.

References

1. Kléber AG, Rudy Y. Basic mechanisms of cardiac impulse propagation and associated arrhythmias. Physiol Rev 2004;84:431.
2. Goldberger JJ, Cain ME, Hohnloser SH, et al. American Heart Association; American College of Cardiology Foundation; Heart Rhythm Society. American Heart Association/American College of Cardiology Foundation/Heart Rhythm Society scientific statement on noninvasive risk stratification techniques for identifying patients at risk for sudden cardiac death: a scientific statement from the American Heart Association Council on Clinical Cardiology Committee on Electrocardiography and Arrhythmias and Council on Epidemiology and Prevention. Circulation 2008;118:1497.
3. Berger RD, Kasper EK, Baughman KL, Marban E, Calkins H, Tomaselli GF. Beat-to-beat QT interval variability: novel evidence for repolarization lability in ischemic and nonischemic dilated cardiomyopathy. Circulation 1997;96:1557.
4. Atiga WL, Calkins H, Lawrence JH, Tomaselli GF, Smith JM, Berger RD. Beat-to-beat repolarization lability identifies patients at risk for sudden cardiac death. J Cardiovasc Electrophysiol 1998;9:899.
5. Burattini L, Zareba W. Time-domain analysis of beat-to-beat variability of repolarization morphology in patients with ischemic cardiomyopathy. J Electrocardiol 1999;32(Suppl):166.
6. Heart rate variability. Standards of measurement, physiological interpretation, and clinical use. Task Force of the European Society of

Cardiology and the North American Society of Pacing and Electrophysiology. Circulation 1996;93:1043.

7. Kreuz J, Lickfett LM, Schwab JO. Modern noninvasive risk stratification in primary prevention of sudden cardiac death. J Interv Card Electrophysiol 2008;23:23.

8. Couderc JP, Zareba W, Burattini L, Moss AJ. Beat-to-Beat repolarization variability in LQTS patients with the SCN5A sodium channel gene mutation. Pacing Clin Electrophysiol 1999;22:158.

9. Bloomfield DM, Steinman RC, Namerow PB, et al. Microvolt T-wave alternans distinguishes between patients likely and patients not likely to benefit from implanted cardiac defibrillator therapy: a solution to the Multicenter Automatic Defibrillator Implantation Trial (MADIT) II conundrum. Circulation 2004;110:1885.

10. Weiss JN, Qu Z, Chen PS, et al. The dynamics of cardiac fibrillation. Circulation 2005;112:1232.

11. Abildskov JA, Evans AK, Lux RL, Burgess MJ. Ventricular repolarization properties and QRST area in cardiac electrograms. Am J Physiol 1980;239:H227.

12. Hubley-Kozey CL, Mitchell LB, Gardner MJ, et al. Spatial features in body-surface potential maps can identify patients with a history of sustained ventricular tachycardia. Circulation 1995;92:1825.

13. Plonsey R. A contemporary view of the ventricular gradient of Wilson. J Electrocardiol 1979;12:337.

14. Geselowitz DB. The ventricular gradient revisited: relation to the area under the action potential. IEEE Trans Biomed Eng 1983;30:76.

15. Cuppen JJ, van Oosterom A. Model studies with the inversely calculated isochrones of ventricular depolarization. IEEE Trans Biomed Eng 1984;31:652.

16. van Oosterom A. Solidifying the solid angle. J Electrocardiol 2002;35 (Suppl):181.

17. Hoekema R, Uijen GJ, Stilli D, van Oosterom A. Lead system transformation of body surface map data. J Electrocardiol 1998;31:71.

18. Khaddoumi B, Rix H, Meste O, Fereniec M, Maniewski R. Body surface ECG signal shape dispersion. IEEE Trans Biomed Eng 2006;53 (12 Pt 1):2491.

19. Lux RL, Smith CR, Wyatt RF, Abildskov JA. Limited lead selection for estimation of body surface potential maps in electrocardiography. IEEE Trans Biomed Eng 1978;25:270.

20. Lux RL, Evans AK, Burgess MJ, Wyatt RF, Abildskov JA. Redundancy reduction for improved display and analysis of body surface potential maps. I. Spatial compression. Circ Res 1981;49:186.

21. Abildskov JA, Green LS, Lux RL. Detection of disparate ventricular repolarization by means of the body surface electrocardiogram. In: Zipes DP, Jalife J, editors. Cardiac electrophysiology and arrhythmias. New York, NY: Grune & Stratton; 1985. p. 495.

22. Yasuma F, Hayano J. Respiratory sinus arrhythmia: why does the heartbeat synchronize with respiratory rhythm? Chest 2004;125:683.

23. Hayano J, Yasuma F, Okada A, Mukai S, Fujinami T. Respiratory sinus arrhythmia. A phenomenon improving pulmonary gas exchange and circulatory efficiency. Circulation 1996;94:842.

24. Grossman P, Taylor EW. Toward understanding respiratory sinus arrhythmia: relations to cardiac vagal tone, evolution and biobehavioral functions. Biol Psychol 2007;74:263.

25. Sunagawa K, Maughan WL, Sagawa K. Optimal arterial resistance for the maximal stroke work studied in isolated canine left ventricle. Circ Res 1985;56:586.

26. Asanoi H, Sasayama S, Kameyama T. Ventriculoarterial coupling in normal and failing heart in humans. Circ Res 1989;65:483.

27. Miyano H, Nakayama Y, Shishido T, et al. Dynamic sympathetic regulation of left ventricular contractility studied in the isolated canine heart. Am J Physiol 1998;275(2 Pt 2):H400.

28. Gepstein L, Hayam G, Ben-Haim SA. Activation-repolarization coupling in the normal swine endocardium. Circulation 1997;96: 4036.

29. Yue AM, Betts TR, Roberts PR, Morgan JM. Global dynamic coupling of activation and repolarization in the human ventricle. Circulation 2005;112:2592.

30. Kozmann G, Haraszti K. Importance of body surface potential field representation fidelity: analysis of beat-to-beat repolarization measurements. Anadolu Kardiyol Derg 2007;7(Suppl 1):5.